Asymmetrical domain wall propagation in bifurcated PMA wire structure due to the Dzyaloshinskii-Moriya interaction

J. Kwon, S. Goolaup, W. L. Gan, C. H. Chang, K. Roy, and W. S. Lew

Citation: Appl. Phys. Lett. **110**, 232402 (2017); doi: 10.1063/1.4984750
View online: http://dx.doi.org/10.1063/1.4984750
View Table of Contents: http://aip.scitation.org/toc/apl/110/23
Published by the American Institute of Physics

Asymmetrical domain wall propagation in bifurcated PMA wire structure due to the Dzyaloshinskii-Moriya interaction

J. Kwon,[1,2] S. Goolaup,[1] W. L. Gan,[1] C. H. Chang,[2,a)] K. Roy,[3] and W. S. Lew[1,b)]
[1]*School of Physical and Mathematical Sciences, Nanyang Technological University, 21 Nanyang Link, Singapore 637371, Singapore*
[2]*School of Electrical and Electronic Engineering, Nanyang Technological University, 50 Nanyang Avenue, Singapore 639798, Singapore*
[3]*School of Electrical and Computer Engineering, Purdue University, West Lafayette, Indiana 47907, USA*

(Received 26 December 2016; accepted 18 May 2017; published online 7 June 2017)

Controlling domain wall (DW) motion in complex magnetic network structures is of paramount significance for the development of spin-based devices. Here, we report on the dynamics of a propagating DW in a bifurcated ferromagnetic wire with perpendicular magnetic anisotropy (PMA). The Dzyaloshinskii-Moriya interaction (DMI) in the wire structure induces a tilt angle to the injected DW, which leads to a quasi-selective propagation through the network branch. The DW tilting causes a field interval between DWs to arrive at Hall bars in the individual branches. Micromagnetic results further show that by tailoring the strength of the DMI, the control of DW dynamics in the PMA complex network structures can be achieved. *Published by AIP Publishing.*
[http://dx.doi.org/10.1063/1.4984750]

Domain wall (DW) propagation is one of the methods for local magnetization switching in memory and logic device applications.[1–3] For enabling higher density devices, perpendicular magnetic anisotropy (PMA) materials are being investigated, as narrow DW structures such as Bloch and Néel configurations are stable.[4–7] The asymmetric film stack constituting the PMA material has been shown to lead to an interfacial Dzyaloshinskii-Moriya interaction (DMI)[8,9] wherein a Néel DW configuration is favored.[10,11] DMI stabilized Néel DW has been reported to have higher speed as the Walker breakdown is shifted to higher external fields.[12–16] For current-driven DW motion, the Néel DW motion in the PMA wire is governed by a combination of DMI and Spin Hall Effect.[17–20] Spin configuration and effective torques acting on the Néel DW play a decisive role in the motion of the DW in the structure.[21,22] Depending on the chirality of the Néel DW, the motion of the DW can be along or against the flow of the current. The DMI stabilized Néel DW configuration has been shown to propagate via a tilting of the DW surface. The DW tilting drives a dynamical effect of magnetization spin configuration of the moving DW in the system. The DMI induced DW tilting has been reported to lead to a depinning anomaly in nanowires with potential barriers. In network structures, the geometrical construction induces an intrinsic potential barrier for DW propagation along the wire. To date, the experimental investigation of DW dynamics in a device with complex geometry remains elusive.[23,24]

In this letter, we report on the dynamics of a Néel DW in a bifurcated nanowire. A single DW is injected into the structure, and its propagation is directly probed by using a combination of Kerr microscopy and anomalous Hall effect (AHE) measurements. Our results reveal that an incoming DW splits at the bifurcation, and the separated DWs propagate asymmetrically at each of the branches due to the influence of DMI.

Multilayered thin film stacks Ta (5 nm)/Pt (5 nm)/[Ni (0.25 nm)/Co (0.5 nm)]$_{\times 4}$/Co (0.5 nm) with a Ta (5 nm) capping layer were deposited on Si/SiO_2 substrates using the sputtering deposition technique. The stack structure is asymmetric with respect to the spin Hall angle of the bottom Pt and the top Ta layer.[25] A 2-μm-wide Y-shaped wire structure with a Hall bar at each of the branches was fabricated using a combination of electron beam lithography and Ar+ ion milling techniques. Ta/Cu/Au films were deposited as electrical contact electrodes. Figure 1 shows Kerr microscopy images of the Y-shaped device structure, which comprises of an 8-μm-long straight wire connected to a curved structure with an 8 μm radial curvature. Each branch of the curved structure is labeled as branch 1 (B1) and branch 2 (B2), and the Hall bars that act as a local detector for probing the DW motion are placed at a short distance from the endpoints of the curved structure. Figures 1(a)–1(d) depict the DW propagation in the structure following nucleation of a single DW in the wire, where the differential Kerr imaging technique was applied. The Y-shaped structure was initially saturated with an external field of 3 kOe along the $-z$-orientation. A 50 ns current pulse, $J_{pulse} = 3.6 \times 10^{11}$ A/m^2, was used for the DW injection.[26,27] The current pulse creates a DW as evidenced by the dark contrast next to the injection line, as seen in Fig. 1(a). Upon applying a driving field of +95 Oe, the injected up-down DW reaches the junction, as shown in Fig. 1(b). The domain expands asymmetrically in both branches, resulting in a DW in each individual branch, as shown in Figs. 1(c) and 1(d). Each DW in the respective branches, B1 and B2, has been observed to reach the Hall bars under different driving field strengths. The DW in B2 required +120 Oe, while that in B1 required +165 Oe. Both DWs exit the ends of the respective branches instantly when a larger driving field, e.g., +185 Oe, was used. This observation is in

a)Electronic mail: echchang@ntu.edu.sg
b)Electronic mail: wensiang@ntu.edu.sg

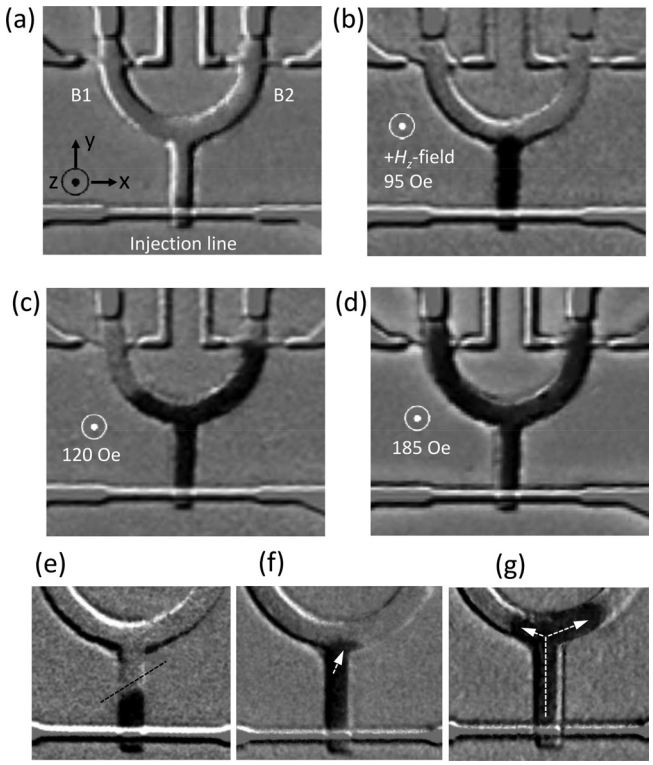

FIG. 1. Kerr imaging of field-induced DW motion in a PMA network structure. (a) A DW nucleated as a current pulse was applied via the injection line. (b) The nucleated DW propagated to the junction of the network structure. (c) and (d) The injected DW splits into two DWs, and each propagated into separate branches, B1 or B2. (e) A close-up of the propagating DW shows a relatively large degree of DW tilting. (f) DW tilt angle has been oriented to the right-handed tilting due to the DW motion in the input wire. (g) The DW tilting gives rise to selective propagation of DWs into each branch.

contrast to the previous report that the splitting of DW always leads to symmetrical DW creation in respective branches.[18] To gain an insight into the splitting process, magnified Kerr images were captured under smaller driving field steps, as depicted in Figs. 1(e)–1(g). The injected DW propagates along the input wire with a tilting in the DW surface. The DW surface has a right-handed tilt orientation with respect to its propagation direction. This type of DW surface tilting is usually stabilized by a DMI vector in the system.[28–30] As can be seen in Figs. 1(f) and 1(g), the DW exhibits a right hand tilt. At the bifurcation, the leading edge of the DW propagates into the right hand branch. Further field leads to a favored direction of the DW in the curved branch. In Figs. 1(e)–1(g), the bright contrast and the dark contrast at the edges of the nanowire along the left-hand branch are the result of measurement artefacts, such as aberration and shadowing effects, which is one of the limitations of our experimental setup. This is especially significant due to the curved edge of the nanowire in the U-shaped section. In our setup, the Kerr images are captured and subtracted from a reference Kerr image. For no magnetization change with respect to the reference, the corresponding differential Kerr image results in no magnetic contrast, corresponding to a grey Kerr image. However, any slight misalignment or the displacement of the sample during the experiment results in the shadowing effect observed along the edges of the nanowire.

The effect of DMI on the DW splitting at the junction was investigated by micromagnetic simulation. The micromagnetic simulations were performed using the object-oriented micromagnetic framework (OOMMF) program.[31] The structure was discretized with a cell size of $5\,\text{nm} \times 5\,\text{nm} \times 3.5\,\text{nm}$. The chosen material parameters are as follows: saturation magnetization, $M_s = 750\,\text{A/m}$; exchange stiffness, $A = 1 \times 10^{11}\,\text{J/m}$; damping parameter, $\alpha = 0.3$; and anisotropy constant, $K_{perp} = 4.8 \times 10^5\,\text{J/m}^3$. To ensure that DW tilting is observed in the simulation, a DMI constant $D = -1.2\,\text{mJ/m}^2$ (Refs. 32 and 24) is chosen. As the DW tilting in our measurement does not appear right after the DW nucleation, the initial configuration of the DW in the simulation is set as Bloch. The DMI subsequently stabilizes a Néel configuration with the up-down DW with internal spin pointing along the left (↑←↓) or the down-up DW with internal spin pointing along the right (↓→↑) as a function of the initial magnetization direction. A schematic representation of a left-handed Néel domain wall propagating in the structure is shown in Fig. 2(a). As the DW propagates towards the junction, the DW leading surface is pinned at the bifurcation edge, a curved profile is subsequently developed as the DW surface reaches the junction, and the up-down DW splits into the two branches eventually. The simulated spin configurations are shown in Fig. 2(b-①∼⑤). The simulation shows that the asymmetric DW expansion at each branch is due to the tilting of up-down Néel wall configuration. As the reversed domain expands within the junction, the DW within branch B2 restores the right hand-tilt and propagates within the branch. For branch B1, a slightly different process is observed.

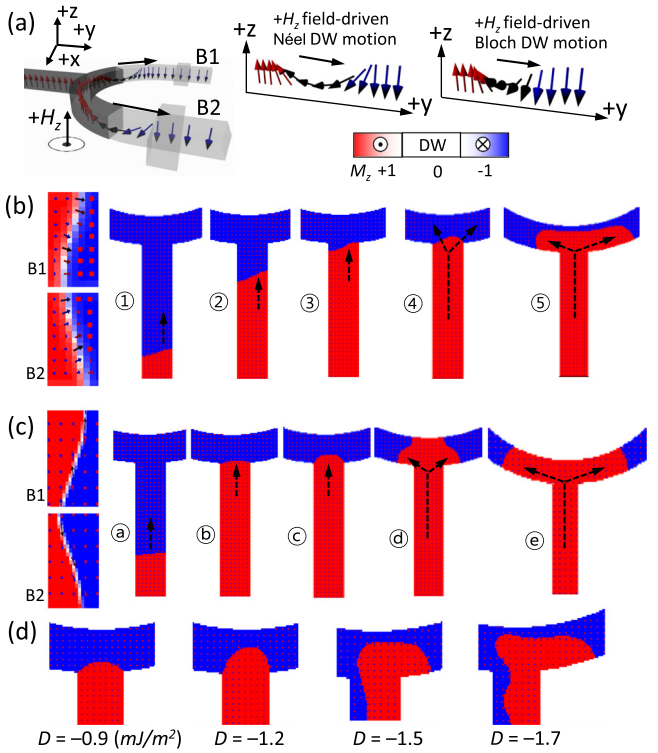

FIG. 2. (a) Schematic illustration of a chiral Néel wall motion in the network structure: a comparison of the chiral Néel and Bloch wall configurations. (b) Simulated propagation of an up-down right-handedness Néel wall in the structure. ①–③ The right-handed tilting DW due to the effect of DMI. ④–⑤ Asymmetrical DW propagation into the network branch. (c) Simulated Bloch wall configuration and propagation in the structure. The Bloch wall motion without the DMI is performed in the simulation in figures labeled ⓐ−ⓔ. (d) Evolution of DW configuration at the junction as the DMI value is varied from $-0.9\,\text{mJ/m}^2$ to $-1.7\,\text{mJ/m}^2$.

Following the depinning at the junction, the DW within branch B1 does not have the requisite right-hand tilt as imposed by the DMI. As such, the DW undergoes a structural re-orientation of the spins to adopt the right-hand tilt. The spin configurations are presented in the supplementary material. This process undeniably slows down the DW propagation through branch B1 while requiring additional external energy for DW stabilization. The asymmetrical DW motion in the structure is consistent with the Kerr microscopy observations and a larger external field required to have the DW in branch B1 reaching the end of the wire.

To understand further the influence of the DMI on the observed phenomenon, we repeated a similar simulation but excluded the DMI factor, i.e., $D = 0$, and the simulated spin configurations are shown in Fig. 2(c). A Bloch wall is stabilized within the system, and no distinct DW surface tilting is observed. At the junction, the propagated Bloch wall expands symmetrically within the bifurcation, and the two separated DWs move into the branches in a near symmetric behavior, as shown in Fig. 2(c-ⓐ–ⓔ). The selective propagation resulting from the DW tilting was further investigated in the simulation by varying the DMI constant. Shown in Fig. 2(d) are the simulated spin configurations as the DW reaches the bifurcation for different values of D. For $|D| = 0 \rightarrow 0.9\,\mathrm{mJ/m^2}$, a DW expands symmetrically in both branches at the bifurcation. By further increasing $|D|$ to 1.2 $\mathrm{mJ/m^2}$, the tilt angle of the right-handed DW increases significantly, and asymmetrical DW propagation is observed at the junction. For $|D| \geq 1.5\,\mathrm{mJ/m^2}$, the stronger DMI causes distortion and elongation to the DW profile, and selective propagation in the branch is no longer present. Interestingly, the measured DMI in the film stack for our devices is ~0.3 $\mathrm{mJ/m^2}$. The asymmetric DW motion within the branch is attributed to the enhanced DW tilting induced by the intrinsic edge roughness in the patterned devices, as can be seen in the Kerr images shown in Fig. 1.

AHE measurements were performed to further investigate the DW dynamics in the network structure.[33,34] The R_{xy}–H_z curves shown in Figs. 3(a) and 3(b) were obtained by using the following sequence: (1) a +3 kOe saturation magnetic field was applied along the $+z$ direction; (2) injection of a down-up DW via a 0.89 V current pulse along the injection line; and (3) measurement of the Hall resistances (R_{xy}) while sweeping the field, and the current is applied through the curved structure. The DW motion can be detected via the R_{xy} changes at the Hall bars. In the structure consisting of a heavy metal and ferromagnetic layer stack, the current induced magnetization dynamics have been suggested to be mediated by the spin orbit torque (SOT) effect.[35–39] The nominal R_{xy} values in the AHE hysteresis loop are used as reference values for down and up magnetized states within B1 and B2 in Figs. 3(a) and 3(b), respectively. The R_{xy} values relevant to the initial up and down magnetized states are obtained as $R_{xy,up} \approx 11.55\,\Omega$ and $R_{xy,down} \approx 10.25\,\Omega$, respectively. The R_{xy}–H_z curve with the up-down DW shows an R_{xy} change at pinning fields of, –180 Oe and –124 Oe at Hall bars B1 and B2, respectively. This result gives a pinning field interval of 56 Oe for the two DWs reaching their respective Hall bars. The obtained DW pinning field values are consistent with the observations of Kerr imaging. To ascertain the reproducibility of the asymmetric DW propagation in the Y-shaped structure, the DW motion in various patterned structures with a width of 2 μm was investigated via the anomalous Hall effect (AHE) voltage detection. For each device, the measurement was repeated ~10 times, and the DW pinning fields in the respective branches were recorded.

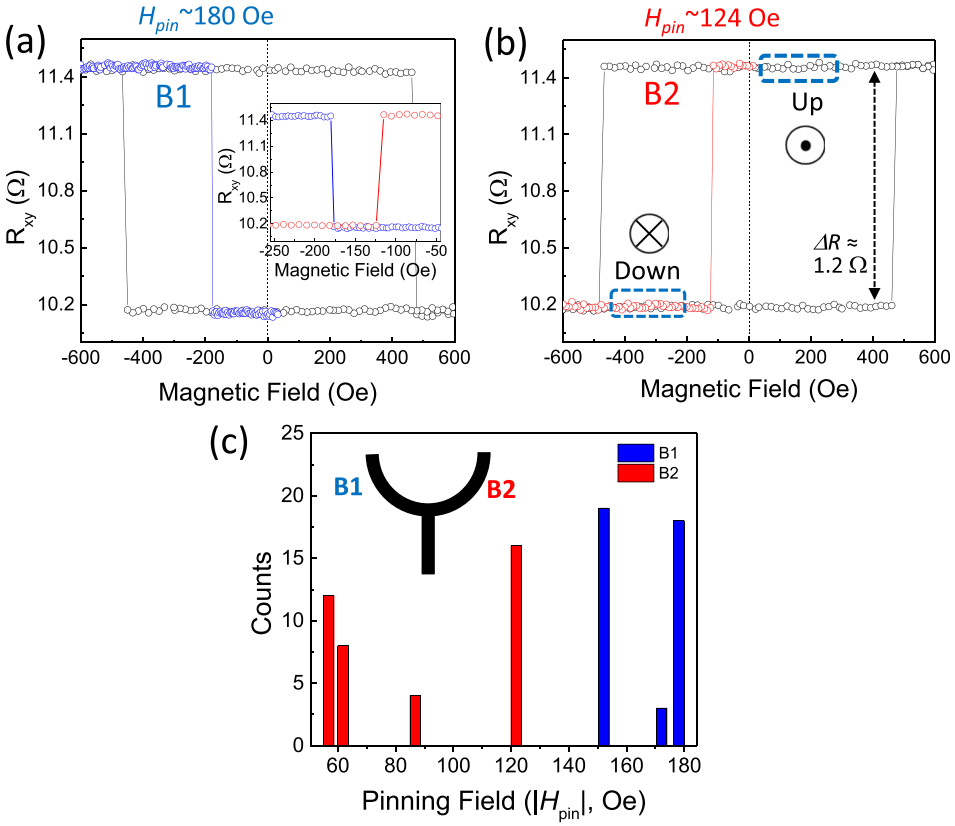

FIG. 3. Hysteresis reversal at each of the branch under the field and current-driven magnetization. (a) and (b) R_{xy} changes in AHE measurement for the pinning field at each of the branch before (black circle line) and after (blue, red circle line) DW creation. The inset shows a comparison of pinning fields due to the DW motion at B1 and B2. (c) Histogram of the pinning fields for 4 devices with 2 μm structures extracted from AHE loops for branches B1 and B2. For each device, the experiment was conducted around 10 times.

Shown in Fig. 3(c) is a histogram of the pinning field for branches B1 and B2 of four different devices investigated. A clear demarcation between the pinning fields between branches B1 and B2 can be clearly observed. The switching in B1 occurs within the field range, $150\,\text{Oe} \leq H_{\mathbf{pin,B1}} \leq 180\,\text{Oe}$, whereas for B2, the pinning field range is $55\,\text{Oe} \leq H_{\mathbf{pin,B2}} \leq 125\,\text{Oe}$. The large range for the pinning field of branch B2, $H_{\mathbf{pin,B2}}$, is attributed to the edge defects playing a prominent role in the DW motion along the wire at low external fields. The pinning field at branch B2 consistently displayed a lower magnitude. As such, the DW within the Y-shaped structure always propagates asymmetrically at the junction. We also repeated the measurement with the smaller wire width, i.e., 500 nm, and a similar depinning field difference for branches B1 and B2 was obtained. The results are presented in the supplementary material.

The DW propagation directions of a left-handed Néel DW with down-up or up-down configuration as a function of the magnetic field or current are illustrated in Fig. 4(a). For field driven dynamics, the DW motion is determined by the expansion/shrinking of domains with respect to the applied out-of-plane field strength. For the down-up Néel DW at position I, the DW moves along the current flow ($+x$-direction), shrinking the "Up" bit within the region bounded by I-II. The externally applied field, Hz, applied along the $+$z (Up) orientation, will expand the $+M_z$ components within the region bounded by I-II. As such, the field induced down-up Néel DW at position I will move along the $-x$-direction. Thus, at position I, the DW motion is governed by an interplay between the current and field induced DW motion. At position II, both the current and field induce the Up-Down Néel DW to move along the current flow ($+x$-direction), expanding the region with $+M_z$ components. In the case of current-driven dynamics, the left handed down-up DW moves along the current orientation. Current passing through the wire structure leads to spin accumulation at the interface between the heavy metals (Pt and Ta) and ferromagnet ($[\text{Co/Ni}]_{\times 4}$).[40,41] The measured SOT effective fields[42–44] in the Hall bar structure with the Pt/$[\text{Co/Ni}]_{\times 4}$ layer are quantified as a function of current density (see the supplementary material). The corresponding Slonczewski-like (SL) and field-like (FL) effective fields are evaluated to be $\sim \pm 25$ Oe at $J_{ac} \approx +5 \times 10^{10}\text{A/m}^2$.

For the current-driven motion of injected down-up and up-down DWs, the R_{xy} change relevant to the current was investigated as the current is swept at ± 4 mA via B2. The respective R_{xy} values for initial down and up magnetized states along the $-z$ and $+z$ orientations are shown in Figs. 4(b)–4(e). Following the injection of an up-down DW at the input wire, the R_{xy} change in branch B2 for the down magnetized state is found to be in the range of $\Delta R_{xy,down} \approx 9.85 \sim 10.25\,\Omega$. A value of $\Delta R_{xy} \approx \pm 0.4\,\Omega$, corresponding to the presence of the DW at the Hall bar, is obtained, as shown in Figs. 4(b) and 4(c). For current flowing along the $+y$ orientation in B2, Fig. 4(b-①), R_{xy} does not change. This implies that the up-down DW may be either moving away from the Hall bar or the current does not induce any DW motion. An abrupt change in R_{xy} is observed in Fig. 4(b-②), as the current is swept along the –y direction, implying that the DW has crossed the Hall bar. When the current is swept back towards the $+$y direction, an abrupt R_{xy} change is observed in Fig. 4(b-④). A schematic depicting the DW dynamics as a function of the applied current is shown in Fig. 4(b). The up-down DW moves opposite to the direction of the applied current.

For the down-up DW, the corresponding magnetization state resistance was found to vary within the range of $R_{xy,up} \approx 11.1 \sim 11.4\,\Omega$, with a value of $\Delta R_{xy} \approx +0.3$ and $-0.4\,\Omega$ for a down-up DW motion, as shown in Figs. 4(d) and 4(e). Interestingly, for the same current sweep, the R_{xy} change occurs at different orientations of current flow. The DW motion as a function of the current is illustrated in Fig. 4(e). As can be seen from Fig. 4(e), the DW motion is along the current flow direction, which is opposite to the current induced dynamics of the up-down DW. These results indicate that the DW propagation direction is strongly dependent on the configuration of the DW rather than the applied current direction in the structure. This is consistent with the SOT induced motion of the chiral Neel DW with right-handedness. The motion of the right handed up-down Neel DW is always accompanied by

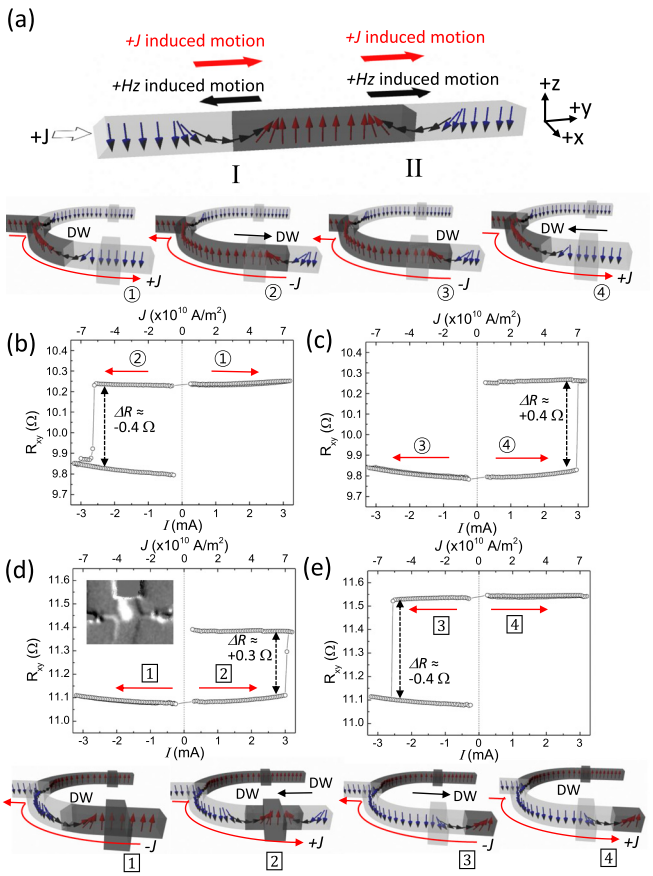

FIG. 4. Detection of current-driven DW motion at the B2 Hall bar. The change in R_{xy} can indicate up-down and down-up DWs in the up ($+H_z$) and down ($-H_z$) magnetized states, respectively. (a) Illustration of left-handed Néel DW motion in the field and current-driven propagation. (b) The illustration shows the relationship between a DW motion and the applied current direction, labeled as ①–④ in B2. First, R_{xy} switching is in the negative current direction (②) with the down-up DW in the initial $-H_z$ magnetized state as current is swept. (c) R_{xy} switching is in the positive current direction (④) as current is swept in the initial $-H_z$ magnetized B2 state. (d) R_{xy} switching is in the positive current direction (2) as current is swept in the initial $+H_z$ magnetized state. (e) R_{xy} switching in the negative current direction (3). The corresponding relationship between a DW motion and the applied current direction is illustrated in 1–4.

a right hand surface tilt of the DW. This is consistent with the Kerr imaging results presented in Fig. 1.

In summary, the direct observation of the DW dynamics in a bifurcated wire reveals that the propagation is via the splitting of DW at the junction, resulting in a DW in each branch. The DMI induced DW tilting leads to quasi-selective propagation through the network structure, with the favored branch determined by the tilting angle of the DW surface. This results in the DW in the individual branches having different depinning fields. Our work shows that by tuning the DMI constant in a material, selective DW motion through a network can be achieved.

See supplementary material for the deterministic DW creation, SOT measurement, and DW propagation at the bifurcation.

This work was supported by a MOE-AcRF Tier 2 Grant (MOE 2013-T2-2-017). Grant support from Singapore National Research Foundation, Prime Minister's Office, under a Competitive Research Programme (Non-volatile Magnetic Logic and Memory Integrated Circuit Devices, NRF-CRP9-2011-01), and an Industry-IHL Partnership Program (No. NRF2015-IIP001-001) is also acknowledged. W.S.L. is a member of the Singapore Spintronics Consortium (SG-SPIN).

[1]D. A. Allwood, G. Xiong, C. C. Faulkner, D. Atkinson, D. Petit, and R. P. Cowburn, Science **309**, 1688 (2005).
[2]D. A. Allwood, G. Xiong, M. D. Cooke, C. C. Faulkner, D. Atkinson, N. Vernier, and R. P. Cowburn, Science **296**, 2003 (2002).
[3]S. S. Parkin and S. H. Yang, Nat. Nanotechnol. **10**, 195 (2015).
[4]C. Burrowes, A. P. Mihai, D. Ravelosona, J. V. Kim, C. Chappert, L. Vila, A. Marty, Y. Samson, F. Garcia-Sanchez, L. D. Buda-Prejbeanu, I. Tudosa, E. E. Fullerton, and J. P. Attané, Nat. Phys. **6**, 17 (2009).
[5]T. Koyama, D. Chiba, K. Ueda, K. Kondou, H. Tanigawa, S. Fukami, T. Suzuki, N. Ohshima, N. Ishiwata, Y. Nakatani, K. Kobayashi, and T. Ono, Nat. Mater. **10**, 194 (2011).
[6]S. S. Parkin, M. Hayashi, and L. Thomas, Science **320**, 190 (2008).
[7]S. H. Yang, K. S. Ryu, and S. S. Parkin, Nat. Nanotechnol. **10**, 221 (2015).
[8]I. E. Dzyaloshinskii, Sov. Phys. JETP **5**, 1259 (1957).
[9]T. Moriya, Phys. Rev. **120**, 91 (1960).
[10]A. Fert, V. Cros, and J. Sampaio, Nat. Nanotechnol. **8**, 152 (2013).
[11]N. Perez, E. Martinez, L. Torres, S. H. Woo, S. Emori, and G. S. D. Beach, Appl. Phys. Lett. **104**, 092403 (2014).
[12]K. J. Kim, Y. Yoshimura, T. Okuno, T. Moriyama, S. W. Lee, K. J. Lee, Y. Nakatani, and T. Ono, APL Mater. **4**, 032504 (2016).
[13]A. Thiaville, S. Rohart, É. Jué, V. Cros, and A. Fert, EPL (Europhys. Lett.) **100**, 57002 (2012).
[14]I. M. Miron, T. Moore, H. Szambolics, L. D. Buda-Prejbeanu, S. Auffret, B. Rodmacq, S. Pizzini, J. Vogel, M. Bonfim, A. Schuhl, and G. Gaudin, Nat. Mater. **10**, 419 (2011).
[15]S. Emori, U. Bauer, S. M. Ahn, E. Martinez, and G. S. Beach, Nat. Mater. **12**, 611 (2013).
[16]E. Martinez, J. Phys.: Condens. Matter. **24**, 024206 (2012).
[17]A. V. Khvalkovskiy, V. Cros, D. Apalkov, V. Nikitin, M. Krounbi, K. A. Zvezdin, A. Anane, J. Grollier, and A. Fert, Phys. Rev. B **87**, 020402 (2013).
[18]K. S. Ryu, S. H. Yang, L. Thomas, and S. S. Parkin, Nat. Commun. **5**, 3910 (2014).
[19]I. M. Miron, K. Garello, G. Gaudin, P. J. Zermatten, M. V. Costache, S. Auffret, S. Bandiera, B. Rodmacq, A. Schuhl, and P. Gambardella, Nature **476**, 189 (2011).
[20]P. P. Haazen, E. Mure, J. H. Franken, R. Lavrijsen, H. J. Swagten, and B. Koopmans, Nat. Mater. **12**, 299 (2013).
[21]M. Bode, M. Heide, K. von Bergmann, P. Ferriani, S. Heinze, G. Bihlmayer, A. Kubetzka, O. Pietzsch, S. Blügel, and R. Wiesendanger, Nature (London) **447**, 190 (2007).
[22]S. Meckler, N. Mikuszeit, A. Pressler, E. Y. Vedmedenko, O. Pietzsch, and R. Wiesendanger, Phys. Rev. Lett. **103**, 157201 (2009).
[23]C. K. Safeer, E. Jue, A. Lopez, L. Buda-Prejbeanu, S. Auffret, S. Pizzini, O. Boulle, I. M. Miron, and G. Gaudin, Nat. Nanotechnol. **11**, 143 (2015).
[24]D. S. Han, N. H. Kim, J. S. Kim, Y. Yin, J. W. Koo, J. Cho, S. Lee, M. Klaui, H. J. Swagten, B. Koopmans, and C. Y. You, Nano Lett. **16**, 4438 (2016).
[25]C.-F. Pai, L. Liu, Y. Li, H. W. Tseng, D. C. Ralph, and R. A. Buhrman, Appl. Phys. Lett. **101**, 122404 (2012).
[26]T. Phung, A. Pushp, L. Thomas, C. Rettner, S. H. Yang, K. S. Ryu, J. Baglin, B. Hughes, and S. S. Parkin, Nano Lett. **15**, 835 (2015).
[27]L. San Emeterio Alvarez, K. Y. Wang, S. Lepadatu, S. Landi, S. J. Bending, and C. H. Marrows, Phys. Rev. Lett. **104**, 137205 (2010).
[28]K.-S. Ryu, L. Thomas, S.-H. Yang, and S. S. Parkin, Appl. Phys. Express **5**, 093006 (2012).
[29]E. Martinez, S. Emori, N. Perez, L. Torres, and G. S. D. Beach, J. Appl. Phys. **115**(21), 213909 (2014).
[30]O. Boulle, S. Rohart, L. D. Buda-Prejbeanu, E. Jue, I. M. Miron, S. Pizzini, J. Vogel, G. Gaudin, and A. Thiaville, Phys. Rev. Lett. **111**, 217203 (2013).
[31]M. Donahue and D. G. Porter, *OOMMF User's Guide, Version 1.0. Interagency Report NISTIR 6376* (National Institute of Standards and Technology, 1999).
[32]A. Hrabec, N. A. Porter, N. A. A. Wells, M. J. Benitez, G. Burnell, S. McVitie, D. McGrouther, T. A. Moore, and C. H. Marrows, Phys. Rev. B **90**, 020402(R) (2014).
[33]R. Lavrijsen, J. H. Franken, J. T. Kohlhepp, H. J. M. Swagten, and B. Koopmans, Appl. Phys. Lett. **96**(22), 222502 (2010).
[34]D. Bhowmik, M. E. Nowakowski, L. You, O. Lee, D. Keating, M. Wong, J. Bokor, and S. Salahuddin, Sci. Rep. **5**, 11823 (2015).
[35]K. Garello, C. O. Avci, I. M. Miron, M. Baumgartner, A. Ghosh, S. Auffret, O. Boulle, G. Gaudin, and P. Gambardella, Appl. Phys. Lett. **105**, 212402 (2014).
[36]K. S. Ryu, L. Thomas, S. H. Yang, and S. S. Parkin, Nat. Nanotechnol. **8**, 527 (2013).
[37]A. Brataas, Nat. Nanotechnol. **8**, 485 (2013).
[38]S. Emori, E. Martinez, K.-J. Lee, H.-W. Lee, U. Bauer, S.-M. Ahn, P. Agrawal, D. C. Bono, and G. S. D. Beach, Phys. Rev. B **90**, 184427 (2014).
[39]I. M. Miron, G. Gaudin, S. Auffret, B. Rodmacq, A. Schuhl, S. Pizzini, J. Vogel, and P. Gambardella, Nat. Mater. **9**, 230 (2010).
[40]M. Hayashi, J. Kim, M. Yamanouchi, and H. Ohno, Phys. Rev. B **89**, 144425 (2014).
[41]A. V. Khvalkovskiy, K. A. Zvezdin, Y. V. Gorbunov, V. Cros, J. Grollier, A. Fert, and A. K. Zvezdin, Phys. Rev. Lett. **102**, 067206 (2009).
[42]H. R. Lee, K. Lee, J. Cho, Y. H. Choi, C. Y. You, M. H. Jung, F. Bonell, Y. Shiota, S. Miwa, and Y. Suzuki, Sci. Rep. **4**, 6548 (2014).
[43]S. Li, S. Goolaup, J. Kwon, F. Luo, W. Gan, and W. S. Lew, Sci. Rep. **7**, 972 (2017).
[44]M. Ramu, S. Goolaup, W. L. Gan, S. Krishnia, G. J. Lim, and W. S. Lew, Appl. Phys. Lett. **110**, 162402 (2017).